Title	Modeling wall film formation and vaporization of a gasoline surrogate fuel
Author(s)	Kobashi, Yoshimitsu; Zama, Yoshio; Kuboyama, Tatsuya
Citation	International journal of heat and mass transfer, 147, 119035 https://doi.org/10.1016/j.ijheatmasstransfer.2019.119035
Issue Date	2020-02
Doc URL	https://hdl.handle.net/2115/83975
Rights	© <2020>. This manuscript version is made available under the CC-BY-NC-ND 4.0 license http://creativecommons.org/licenses/by-nc-nd/4.0/
Rights(URL)	https://creativecommons.org/licenses/by-nc-nd/4.0/
Type	journal article
File Information	Manuscript_w_Figure_Table.pdf

Modeling Wall Film Formation and Vaporization of a Gasoline Surrogate Fuel

Yoshimitsu Kobashi[1]*, Yoshio Zama[2] and Tatsuya Kuboyama[3]

[1] Graduate School of Engineering, Hokkaido University, Japan

[2] Graduate School of Science and Technology, Gunma University, Japan

[3] Graduate School of Engineering, Chiba University, Japan

Abstract

To simulate the wall film formation and vaporization processes in gasoline direct-injection spark-ignition engines including considerations of the physical properties and vapor-liquid equilibrium of multi-component fuels, spray-wall interaction sub-models were implemented with the 3D-CFD software HINOCA which has been developed for automotive engine cylinder simulations. The models used were the Senda model for spray-wall impingement including splash, deposition, droplet-droplet interactions, and droplet-film interactions; the O'Rourke model for heat transfer and film vaporization; a simple film flow model considering momentum conservation; and Raoult's law for vapor-liquid equilibrium. First, the model validated the calculated results for a single-component fuel (iso-octane) through comparisons with experimental data in terms of wall film area and heat flux between the wall and film. Second, numerical simulations were conducted with a 5-component gasoline surrogate fuel which was designed taking into account the average octane number, aromatic content, and distillation characteristic. The results showed clear differences in the contributions of the 5 components to the wall film, and the possibility that the aromatic content with higher carbon atoms could be a source of soot formation.

Keywords: Gasoline Direct Injection Engine, Wall Film, Spray, Gasoline Surrogate Fuel

Nomenclature:

A	Area [m^2]
d	Diameter of droplet [m]
E	Kinetic energy of droplet or wall film [J]

---

* Corresponding author at: Kita 13, Nishi 8, Kita-ku, Sapporo, Hokkaido, Japan

E-mail address: kobashi@eng.hokudai.ac.jp (Y. Kobashi)

E_{crit}	Energy needed to break up droplet [J]
K	Critical parameter which correlates deposition and splash [-] ($= Z\cdot Re^{1.25}$)
La	Laplace number [-]
m	Mass of droplet or wall film [kg]
M	Total mass [kg]
Oh	Ohnesorge number [-] ($= \sqrt{We}/Re$)
p	Pressure [Pa]
$\dot{Q}$	Heat flux [W/m^2]
Re	Reynolds number [-]
t	Time [s]
t_r	Time interval parameter [-] ($= \Delta t/\tau_{\mathrm{res}}$)
T	Temperature
v	Velocity of droplet or wall film [m/s]
We	Weber number of droplet [-]
y	Mass fraction [-]

Subscripts:

1	Before impingement on wall
2	After impingement on wall
$crit$	Critical
f	Wall film
g	Gas
i	Component
inj	Injection
l	Liquid
n	Normal to wall
s	Surface of wall film
t	Tangential to wall
w	Wall

Greek symbols:

δ	Film thickness [m]
δ_N	Non-dimensional film thickness ($= \delta/d_{\mathrm{p}}$) [-]
Δt	Time interval between two continuous droplets reaching a wall [s]
φ	Equivalence ratio [-]
λ	Thermal conductivity [W/(m·K)]
μ	Viscosity [Pa· s]
ρ	Density [kg/m^3]
σ_l	Surface tension of liquid [N/m]
τ_{air}	Shear force between airflow and wall film [Pa]

τ_{res}	Droplet residence time on wall [s]
τ_w	Friction stress between wall film and wall [Pa]

1. Introduction

Due to the improvements in thermal efficiency and engine power output, modern gasoline engines have employed direct-injection spark-ignition (DISI) systems. In this strategy, however, soot may be produced as the result of the formation of a liquid film (wall film) on the piston surface and from pool fires fed by the wall film [1][2]. To develop DISI engines which avoid the wall film formation and reduce the mass and number of soot particulate, it is crucial to develop numerical analysis schemes that treat the spray-wall interaction, film flow, and film vaporization processes in more detail, as well as to develop an understanding of the source of the soot particles.

Over the past decades, a number of spray-wall impingement models have been developed. Naber and Reitz [3] proposed one of the first impingement models, which considers three regimes including stick, rebound, and slide of the impinged droplets. Bai and Gosman [4] proposed a more detailed model which includes wider impingement regimes; adhesion (stick and spread) and splash for dry walls; rebound, spread, and splash for wetted walls, while employing We_{crit} as the critical Weber number for regime transition criterion. Stanton and Rutland [5], assuming wetted walls, also derived a model in which We_{crit} was used as the critical criterion of the regime transition. A single-droplet experiment by Mundo et al. showed that the limit of adhesion and splash can be correlated in terms of the Reynolds number Re and the Ohnesorge number Oh, and an additional critical parameter K ($= Oh \cdot Re^{1.25}$) was also introduced [6]. The recent study [7] has demonstrated that using Kuhnke's spray-wall interaction model [8], in which the effects of the critical parameter K and a thermal parameter defined as the ratio of the wall temperature and the droplet boiling temperature are considered, a good agreement of wall film height distributions between the measurements and calculations. Zhang et al. proposed a model considering the droplet/film interaction on the film dynamics, and the dissipative energy loss during the expansion of the lamella formed by the deformation of the deposited droplet [9]. Senda et al. [10-11] proposed a more comprehensive model which considers the effects of the Weber number We and liquid film thickness on spray-wall interaction behaviors as well as a We_{crit} parameter as the regime transition criterion.

For wall film vaporization, the model developed by O'Rourke and Amsden [12] is reliable and often used in the literature, as it consists of physical processes like the wall film energy balance, heat transfer from the wall to the film and to the impinging droplets, and the temperature profile in the film normal to the surface. Recently, Jiao and Reitz employed the model to simulate the soot formation from the wall film in a DISI engine [13]. Another important aspect in the wall film vaporization is the distillation characteristics of fuels as gasoline is multicomponent fuel, and the component remaining in the wall film has a significant impact on the soot formation, like for example, many of high boiling point gasoline components are aromatics [14] which tend to increase soot emissions. A number of vaporization models have been developed for multicomponent fuels [15-21]. However, there have been few studies that conducted extensive validation of the models including the film evaporation process and heat flux between the wall and wall film, although the heat flux modeling was studied well for single component liquid [9, 22]. In addition, little has been reported on the correlation between the vaporization process of wall films and the distillation characteristics of fuels. Köpple et al. proposed a gasoline surrogate fuel consisting of n-hexane, iso-octane and n-decane [23]. Using this surrogate fuel, Köpple et al. validated the heat transfer between the piston wall and wall film [7], and showed a good correlation between the calculated mixture formation and the measured particulate emissions [23]. Schulz and Beyrau demonstrated that this gasoline surrogate fuel represents the wall film vaporization of real gasoline [24].

The purpose of the present study is to develop a simulation scheme that predicts the wall film formation and vaporization of multicomponent fuel sprays with a high degree of accuracy, and to investigate the potential source of soot in DISI gasoline engines. Sub-models accommodating this were incorporated into the platform software HINOCA [25]. The calculated wall film area and heat flux between the wall and wall film in this study were validated via comparisons with data obtained by measurements developed specially for this study, followed by modifications to the sub-models. A gasoline surrogate fuel was designed to meet the average octane number, aromatic contents, and distillation characteristic of real gasoline fuel. Finally, the correlation between the formation and vaporization processes of wall films and the components of the gasoline surrogate fuel was examined.

2. Model description

The platform software employed in this study is HINOCA [25] which is an automotive engine cylinder simulation software, based on fully compressible Navier-Stokes equations which are filtered for Large Eddy Simulation (LES), and employs Cartesian grid and immersed boundary (IB) methods. The grid is set to be equally spaced for simplicity of the code. The wall adapting the local eddy viscosity (WALE) model which is capable of predicting wall limiting behaviors without the calculation of the wall distance [26] is also adopted.

Spray models are based on a DDM (Discrete Droplet Model) which describes spray droplets by stochastic particles that are termed parcels, and spherical parcels having a diameter equal to the nozzle hole are injected. The KH-RT model [27] was used to simulate the primary and secondary breakup processes. When a spray parcel impinges on a wall, it is converted into a wall film parcel. This process was modeled, and here in this following section, where wall film models implemented in HINOCA are introduced.

2.1 Spray-wall impingement model

A number of spray-wall impingement models have been proposed [3-11]. The authors selected a model developed by Senda et al. [10-11] as the base model since it is comprehensive with consideration of the effects of the liquid film (wall film) thickness, and the diameter and Weber number of the impinging droplets $We_{1,n}$ $(= \rho_l \, d_1 v_{1,n}^2/\sigma_l,$ ρ_l : liquid density, d_1 : diameter of droplets impinging on a wall, and, $v_{1,n}$: velocity component of droplets, normal to a wall, with, σ_l : the surface tension). Further, the present study focuses on the wall film formation, and agreement of the wall film shape between the measurements and numerical simulation was demonstrated with the Senda model [28]. Note that the Senda model developed in the literatures [10-11] is only applicable to a limited range of temperatures of droplets and walls, where the boiling-induced breakup is negligible.

Figure 1 (a) summarizes the classification of impinging droplet characteristics in the Senda model, where the non-dimensional film thickness δ_N is defined as the film thickness δ divided by droplet diameter d_1 [10-11]. The model is divided into two regimes based on the Weber number, $We_{1,n}$ of an impinging droplet as shown in Fig.1 (b).

(1) Low Weber number model ($We_{1,n} \leq 300$)

(1-1) Wet wall

Three types of breakup: rim type; cluster type; and column type are considered when a droplet impinges on a wet wall, and the droplet diameter after the breakup d_2 is given as a function of the non-dimensional film thickness δ_N to fit experimental results as follows [29]:

$$d_2/d_1 = 0.6478 - 0.5480\,\delta_N + 1.9825\,\delta_N^2 - 2.1082\,\delta_N^3 + 0.6894\,\delta_N^4 \tag{1}$$

The droplet velocity after the breakup is determined with the Weber number of the bouncing droplet. The relation between the Weber number and non-dimensional film thickness δ_N is determined to fit experimental results as follows [29]:

$$We_{2,t} = 0.3818 - 0.00537\,\delta_N - 0.8937\,\delta_N^2 + 0.8644\,\delta_N^3 - 0.2301\,\delta_N^4 \tag{2-1}$$

$$We_{2,n} = -2.1518 + 1.1493\,\delta_N + 26.238\,\delta_N^2 - 24.480\,\delta_N^3 - 5.5650\,\delta_N^4 \tag{2-2}$$

where $We_{2,t}$ is the Weber number, tangential to a wall, of the bouncing droplet, and $We_{2,n}$ is that normal to a wall.

(1-2) Dry wall

Almost all droplets stick when impinging on a dry wall, but some bounce after the impingement. A subsequent droplet likely collides with the foregoing one, causing breakup of the droplets. The probability of the breakup can be estimated with a time interval parameter, t_r which is defined as follows:

$$t_r = \Delta t/\tau_{res} \tag{3}$$

where Δt is the time interval between the two continuous droplets reaching a wall, and τ_{res} is the droplet residence time on the wall, expressed as follows [30]:

$$\tau_{res} = \pi\sqrt{\rho_l\, d_1^3/(16\sigma_l)} \tag{4}$$

The model defines that the breakup occurs at the t_r from 0.4 to 0.6, where high breakup probabilities were determined in experiments [29]. In the present study, the diameter and velocity of the droplet after the breakup was calculated assigning $\delta_N = 0$ in Equations (1), (2-1) and (2-2).

(2) High Weber number model ($We_{1,n} > 300$)

At $We_{1,n}$ numbers above 300, the model assumes that the droplet impinging on a dry wall causes the breakup while that impinging on a wet wall leads to splashing or deposition in the wall film. The critical Weber number, We_{crit} is used as a criterion that distinguishes splashing from deposition, according to the experimental work of Cossali et al. [31] as follows:

$$We_{crit} = (2100 + 5880\,\delta_N^{1.44})La^{-0.2} \tag{5}$$

where La is the Laplace number ($= \sigma_l \rho_l d_1 / \mu_l^2$, μ_l : liquid viscosity).

The droplet diameter after the breakup and splash is determined according to the experimental data of Mundo et al. as follows [32]:

$$d_2/d_1 = 3.932 \times 10^2 \times K^{-1.416} \qquad \text{(for rough surfaces)} \qquad (6)$$

$$d_2/d_1 = 3.903 \times 10^{10} \times K^{-5.116} \qquad \text{(for smooth surfaces)} \qquad (7)$$

where K is a non-dimensional parameter defined as:

$$K = Oh \cdot Re^{1.25} \qquad (8)$$

with $Oh = \mu_l / \sqrt{\rho_l \sigma_l d_1}$ the Ohnesorge number and $Re = \rho_l d_1 v_{1,n} / \mu_l$ the Reynolds number. This study applied Equation (6) to wet walls, and Equation (7) to dry walls, in analogy with the original model.

The droplet velocity after the wall impingement is critical to determine the velocity of growth of a wall film as will be explained in Equation (12). The original model calculates the velocity while solving the balance between the energy needed to break up the droplet, E_{crit} and the kinetic energies of the droplets before the impingement, E_1 and after the impingement (including droplets becoming part of the liquid film, E_f and being airborne, E_2) as:

$$E_1 - E_{crit} = E_f + E_2 \qquad (9)$$

The film flow calculated with Equation (9), however, was inconsistent with the experimental results in this study. This study then employed the film flow model proposed by Kalantari and Tropea [33] which expresses the droplet velocity after the wall impingement as:

$$v_{2,n}/v_{1,n} = -1.1 \cdot We_{1,n}^{-0.36} \qquad (10)$$

$$v_{2,t} = 0.862 \cdot v_{1,t} - 0.094 \qquad (11)$$

with $v_{2,n}$ the velocity component, normal to a wall, and $v_{2,t}$ that tangential to a wall.

2.2 Film flow model

To calculate the flow characteristics of the wall film, a momentum balance equation was solved. In the model, parcels of injected fuel are deposited on one IB cell which is assumed to form a rigid wall film, and the equation is expressed as:

$$\Delta\left(M_f\vec{v}_f\right) = \sum(m_1\vec{v}_1 - m_2\vec{v}_2) + \vec{\tau}_{air}Adt - \vec{\tau}_wAdt \tag{12}$$

where M_f and $\vec{v}_f$ are the total mass and velocity vectors of the wall film in a cell. The first term on the right side is the momentum provided from impinging droplets to the wall film, with m_1 and m_2 the mass of the droplets before and after impingement. The A is the area of the wall film and is identical with the cross-sectional area of the IB cell. The τ_{air} is the shear force between the airflow and wall film, and the τ_w is the frictional stress between the wall film and wall.

2.3 Film vaporization model

The model proposed by O'Rourke and Amsden [12] was used to calculate the film vaporization and heat transfer to the wall film. This model considers the change in the structure of the turbulent boundary layers above the wall films because of the gas velocity normal to the wall induced by vaporization and consequent convective transport. Two assumptions are made: (1) the total transport is independent of the coordinate normal to the wall and is the sum of the transport due to turbulent diffusion and due to convection by the vaporization velocities; (2) there is a linear increase in the turbulent diffusivity with the distance from the wall.

The temperature profile in the wall film normal to the wall is approximated as linear, varying from the temperature at the wall T_w to the mean temperature T_f in the lower half (the half nearest the wall) of the film, and from T_f to the film surface temperature T_s in the upper half of the film, as schematically suggested in Fig.2, where $\dot{Q}_s$ and $\dot{Q}_w$ are the heat fluxes between the gas and liquid film, and between the liquid film and wall, and λ_l is the thermal conductivity of the liquid. The energy balance is solved considering the heat transfer between the gas and film and the wall and film, and the changes in the temperature resulting from the film movement and droplet impingement.

The mass vaporization rate, $\dot{M}_{vap}$ is given by

$$\dot{M}_{vap} = H_y \ln\left(\frac{1-y_v}{1-y_s}\right) \tag{13}$$

where y_v is the fuel vapor mass fraction, and y_s is the equilibrium vapor mass fraction at the surface temperature. One of the authors (Kobashi) has developed a method for estimating the vapor-liquid equilibrium of vaporizing multicomponent sprays with the Soave-Redlich-Kwong equation of state combined with the UNIFAC method [34], but Raoult's law for an ideal multicomponent mixture was employed for simplicity in this study since the fuels used were with non-polar molecules, and all numerical simulations were implemented at atmospheric pressure.

H_y is expressed as:

$$H_y = \frac{\rho_g u_\tau}{y_c^+ Sc_L + \frac{Sc_T}{\kappa} ln\left(\frac{y^+}{y_c^+}\right)} \qquad \text{if } y^+ > y_c^+$$

$$H_y = \frac{\rho_g u_\tau}{y^+ Sc_L} \qquad \text{if } y^+ < y_c^+ \tag{14}$$

where Sc_L and Sc_T are the laminar and turbulent Schmidt numbers, u_τ is the frictional velocity defined as $u_\tau = (\tau_w/\rho_g)^{0.5}$, $y^+ = y\ u_\tau/\upsilon_L$, y is the distance normal to the wall, τ_w is the wall shear stress, and υ_L is the kinematic viscosity. The transition between the laminar and fully turbulent region, y_c^+ is 11.05, and Karmann's constant, κ is 0.433, according to the literature [12].

The wall film thickness, δ was calculated as follows:

$$\delta = \frac{\sum V_p}{A} \tag{15}$$

where $\sum V_p$ is the sum of the volume of parcels adhering to a wall defined by a Cut-Cell method, and A is the cross-sectional area of the wall.

3. Experimental Setup and Procedures

3.1 Measurement of wall film area

In a constant volume vessel, the temporal development of the wall film area was measured with the refractive index matching (RIM) method which allows photography of the wall films based on the principle that the light transmission decreases when liquid is deposited on a frosted glass wall [2]. A schematic of the experimental system is shown in Fig.3. The fuel was pressurized by the high pressure pump and injected into the vessel in which the frosted glass wall was placed. Use of continuous light emitted from the metal halide lamp (Photron: HVC-UL) and a high speed digital camera (Vision Research: Phantom-MIRO) allowed sequential imaging of deposition and flow of the wall film from the rear of the wall. Electrical signals sent from the pulse generator were utilized to determine the fuel injection period as well as the triggers for the injection and image recording.

The arrangement of the sprays and the wall are shown in Fig.4. The injector was equipped with a 6-hole nozzle. Spray from the No.6 nozzle impinged on the wall at an angle of 23° from a distance of 22 mm, while sprays of the No.2, 3, and 4 nozzles which were in the same plane and impinged at the angle of 45°. As the sprays of the No.1 and 5 nozzles geometrically do not result in wall impingement, the numerical simulations were implemented only for the sprays No.2, 3, 4, and 6. The rear view image in Fig.4 (c) is an example of the RIM image with the numbers of the sprays superimposed near the positions where impingement takes place. The dark areas represent regions where the wall film has formed, while the thicker film is located near the position of spray impingement and appears white as the wall film here became thicker than the surface roughness of the frosted glass.

3.2 Measurement of the wall heat flux

The experimental setup for the measurements of the wall heat flux is shown in Fig.5. As shown in Fig.5 (a), the wall was placed below the injector, and a Loex-bodied thin-film thermocouple developed by Enomoto [35] was embedded in the wall. The body material of the Loex has a density, heat capacity, and heat conductivity closely equivalent to the wall material. The diameter of the body of the thermocouple was 3.0 mm, and the diameter of the electrically-insulated center wire made of constantan was 0.15 mm. A thin copper film, about 10 μm thick, was formed to establish a hot junction of the Loex – constantan with a very low heat capacity on the top surface of the thermocouple, while a cold junction was made inside the body of the thermocouple at the distance of 3.5 mm from the top surface. Another thermocouple, of iron – constantan, was embedded near the cold junction and with the cold junction immersed in ice water. Overall, it was possible to measure the temperature differences between the hot and cold junctions of the Loex – constantan thermocouple and to calculate the wall heat flux as the absolute temperature of the cold junction was measured with the iron – constantan thermocouple. The accuracy of the measurement system has been investigated by Enomoto who reported that the wall heat flux measured was about 5 % higher than the true value [35].

The thermoelectrical power from the thermocouple was amplified and recorded with the data logger. The temperature of the wall surface was controlled with a heater, based on the temperature measured by the iron – constantan thermocouple. The fuel was pressurized with nitrogen gas and introduced to the injector. Electrical signals sent from the pulse generator were used to determine the fuel injection period as well as the triggers for the injection, data logging, and image recording. The wall film images were recorded with the high speed digital camera (NAC: HX-3) and the wall film was illuminated with the metal halide lamp (Photron: HVC-UL), and recorded from a position diagonally above the wall.

Figure 5 (b) shows the layout of the fuel sprays and thermocouple for the measurement of the wall heat flux. The fuel injector equipped with a 6-hole nozzle was different from the one used in the film area measurements. The fuel spray injected from one nozzle hole orthogonally above the wall impinged on the thermocouple embedded in the piston while the other sprays were masked with the metallic plate. The gap between the target spray and metallic plate is large enough, and it was confirmed that the other sprays have a limited impact on the target spray after the wall impingement with the movie.

4. Validation of the Model with iso-Octane

4.1 Wall film area

Table 1 details the conditions under which the wall film areas were compared in the measurement and calculations. A single component fuel, iso-octane (2,2,4-trimethylpentane, iC_8H_{18}) was injected from the 6-hole nozzle with nozzle diameters of 0.13 mm into a constant volume vessel at room temperature and atmospheric pressure. The injection pressure, p_{inj} was changed as the variable.

Figure 6 shows the images of (a) the wall film photographed with the RIM method from the rear of the frosted glass wall, and (b) the calculated wall film thickness, with the injection pressure, p_{inj} of 13 MPa. In Fig.9 (a), the darkly colored areas represent regions where the wall film formed, and the thick film near the location of the spray impingement appear as white. In Fig.7 (b), the overall shape of the calculated wall film is very similar to the photograph, the calculated thicker region presented in red corresponds to the white regions in the measured image. The thicker films formed at the location far from the spray impingement points, and the film thickness other than the thicker region was in the order of 10 μm. These observations are in agreement with film thickness distributions of a literature [36], in which the experimental conditions are similar to the present study.

Figure 7 shows profiles of the wall film area plotted for different injection pressures p_{inj}. Here, the film area in the calculations was defined as the sum of the areas where the film thickness was larger than 1 μm, corresponding to the detectable level in the measurements. The measured results show that the wall film area increased with time until 5.5 ms, and then it maintained a nearly constant size. The higher injection pressure increased the wall film area. The calculations captured the changes in the initial spreading process of the film area, and the fact that the film area increased with increasing injection pressure, however the calculations underestimate the film area at the lower injection pressure. The reason for this discrepancy may be due to underestimation of the impinging droplet diameter at the lower injection pressures, and may be attributed to the droplet breakup model and the critical Weber number.

4.2 Heat flux between the film and wall

The heat flux between the film and wall, $\dot{Q}_w$ would be an appropriate factor to validate the model as it plays an important role in the wall film vaporization as well as because accurate predictions of wall film formation and movement are required in the predictions.

Table 2 details the conditions under which the measured and calculated wall heat flux values were compared. A single component fuel, iso-octane was injected from an injector equipped with a 6-hole nozzle with nozzle diameters of 0.248 mm. The long injection period of 4 ms was adopted to measure the heat flux in a quasi-steady state. The heat flux was measured for one spray impinging on the wall as explained in Section 3.2, while the calculation assumed a single-hole nozzle with the same diameter. In the calculation, the heat flux between the film and wall, $\dot{Q}_w$ was calculated as follows:

$$\dot{Q}_w = \lambda_l \frac{T_f - T_w}{\delta/2} \qquad (16)$$

where λ_l is the liquid thermal conductivity.

Figure 8 shows photographs and calculated images of the wall film at 7 ms after the start of injection where the wall film is in the quasi-steady state. In Fig.8 (a), the photos were taken from the diagonally upward direction at an angle of 45° as shown in Fig.5 (a), making the scale of the picture longitudinally compressed. The calculated images in Fig.8

(b) superimposes dashed circles equivalent to the measured diameter of the wall film. Unlike the situation in Fig.7, the calculations overestimated the wall film spread. This may be due to differences in the wall surface roughness, or due to differences between the effect of the oblique and orthogonal impingements. However, the calculations captured the experimental observation that the edge of the wall film was thicker than the central portion. There was boiling at the center of the wall film in both the (a) photographed and (b) calculated images at T_w of 100ºC which is slightly higher than the boiling point of iso-octane. Further, at the T_w of 120ºC, the boiling was taking place over the whole of the wall film in the photograph (a), and the calculation shows less wall film in (b), indicating that actually most of the wall film had vaporized.

Figure 9 plots the profiles of the heat flux of the measurements and calculations, where the wall temperature, T_w was set at 120ºC. In the calculations, the heat flux was calculated for the region just below the nozzle, considering the area equivalent to the top surface of the thermocouple. The direction of the heat transfer toward the wall was defined as positive. Since the temperature of the fuel spray is lower than the wall temperature, the heat transferred from the wall to the spray or wall film results the negative value. Both the measured and calculated heat fluxes decreased rapidly immediately after the spray impingement, and they gradually increased from 4 ms after the start of injection when no spray reached impingement to the wall. Averaging the heat flux from 1 ms to 2.5 ms after the start of injection, the measured value was -4.1 MW/m^2, with the calculated value -3.5 MW/m^2, a difference of about 15%.

Figure 10 plots the change in the heat flux with the wall temperature T_w as measured and calculated. The heat flux decreased with the increase of the T_w. According to Schulz et al. who determined the transient wall temperature and heat flux at the spray impingement zone using an infrared thermography for an extensive range of influencing factors, the heat fluxes during the spray impact are -3 MW/m^2 at the T_w of 80ºC and -4

MW/m^2 at the T_w of 120°C [37], which correspond to the heat flux measured in the present study. There were the differences in the absolute values of the heat flux between the measurements and calculations, but the decreases with T_w are practically identical, with similar global gradients.

Figure 11 plots the change in the heat flux with the distance from the nozzle to the wall as measured and calculated. The heat flux increased with the increase of the distance. The trend corresponds to the results of Schulz et al. [37], but it has a limited impact on the heat fluxes measured and calculated within the range of the present study.

5. Formation and Vaporization of the Wall Film with a Gasoline Surrogate Fuel

5.1 Specification of the gasoline surrogate fuel

The composition of the gasoline surrogate fuel was determined to meet the octane number, aromatic content, and distillation curve of the regular gasoline available in Japan. It was assumed that the RON (research octane number) can be expressed as a volume-averaged property, and the distillation curve was calculated following a calculation method reported elsewhere [38]. It assumes an open system where the vaporized fuel is vented. The heat, Q is continuously supplied from outside the system to the liquid, and consumed in increasing the temperature up to and vaporizing the liquid. Considering a vapor-liquid equilibrium (VLE), the composition in the liquid and vapor phases is calculated and renewed at every time step, via a VLE calculation with NIST SUPERTRAPP [39] which solves the Peng-Robinson equation of state [40].

Table 3 (a) details the components selected as the composition of the gasoline surrogate fuel, the properties, and the mixing fractions. The five components are needed to reproduce the desired distillation curve. Considering that the aromatics have higher boiling points than a range of other gasoline components [14], 1,2,4-trimethylbenzene

(C_9H_{12}) was chosen as the highest boiling point component, however, iso-butylbenzene ($C_{10}H_{14}$) was used as a substitute in the calculations due to the lack of information on the thermodynamic properties of 1,2,4-trimethylbenzene. Iso-pentane was chosen as the lowest boiling point component since it exhibits low reactivity (high RON), and it is liquid at the conditions involved here and is simple to handle. The medium boiling point components: n-heptane, iso-octane, and toluene, function to adjust the RON and aromatic content.

The properties and distillation curve of the gasoline surrogate fuel are shown in Table 3 (b) and Fig.12. The properties of the surrogate fuel are closely identical to the reference regular gasoline (commonly available in Japan). The distillation curve appears well matched, except for the disagreement at the distillation ratios from 40% to 80% and near the end point.

5.2 Formation and Vaporization of the Wall Film

In this section, first, the accuracy of the present model is evaluated by comparing the film area of the gasoline surrogate fuel as measured and calculated. Second, the vaporization process of a wall film of the gasoline surrogate fuel is discussed with the calculations.

The conditions under which the film area was evaluated are identical with Table 1, with the injector - wall arrangement, that in Fig.3 and 4, except for the wall temperature T_w of 60°C and the fuels tested. The fuel was injected with the pressure of 13 MPa into ambient air at atmospheric pressure.

Figure 13 shows the changes in the calculated film mass distributions of (a) the gasoline surrogate fuel and (b) the iso-octane. For the gasoline surrogate fuel there were no significant observable changes in the distributions of the wall film mass as shown in Fig.13 (a). The wall film vanished from the thinner film with (b) iso-octane since the heat flux inversely increased with the film thickness as expressed in Eq.(16).

Figure 14 plots (a) the measured and calculated area of the wall film and (b) the calculated film mass of the gasoline surrogate fuel and iso-octane at the wall temperature T_w of 60ºC. In Fig.14 (a), the measured film area of iso-octane (red open squares) decreased due to the vaporization noted from 5 ms after the start of injection. The wall film of the gasoline surrogate fuel (blue open circles) show a wider film area than that of iso-octane, which decreased at a slow rate. This tendency matched with the experiment of Schulz [24]. The calculations underestimated the film area of the gasoline surrogate fuel (solid blue line). This is because iso-pentane which is the lowest boiling point component may be assumed to form a vaporized layer on the wall immediately after the wall impingement and this layer reduces the heat flux from the wall to the film in the experiment, a process that was not incorporated in the calculations. Other than this inconsistency, the calculations demonstrate good agreement with the measurements and capture the changes in the vaporization process from 5 ms after the start of injection. The changes in the calculated film mass in Fig.14 (b) reflect the results with the measured changes.

Figure 15 plots the calculated profiles of the mass fraction of the components present in the wall film of the gasoline surrogate fuel. Compared with the original mass fractions detailed in Table 3, it is clear that most of the iso-pentane (solid black plot) vaporized immediately after the wall impingement. For the medium boiling point components: iso-octane (solid blue line), n-heptane (dashed black line), and toluene (solid gray line), the wall temperature T_w of 60ºC is lower than their boiling points, and the vaporization was at slower rates. At 20 ms after the start of injection, the highest boiling point component iso-butylbenzene (dashed red line) formed the largest quantity of the wall film as little had vaporized at the wall temperature here. Considering that the aromatic contents have higher boiling points among a range of gasoline components, they would present the possibility to yield soot, feeding the pool fires occurring in the warm-up operations of

DISI gasoline engines.

6. Conclusions

The present study developed a CFD model to predict the wall film formation and vaporization of multicomponent fuel sprays. The calculated results with the model were validated by a comparison with actual measurements. Finally, the model was used to understand details of the wall film behavior of a gasoline surrogate fuel. The conclusions may be summarized as follows:

1. The calculations with the developed model reproduce the observed trend that the film area increases with increases in the fuel injection pressure.
2. The calculated film thickness at the edge of the wall film is thicker than at the central portion, similar to the observation in the experiments.
3. With iso-octane (boiling point 99.3°C), boiling occurs from the center of the wall film at the wall temperature of 100°C, and the whole wall film boils at the wall temperature of 120°C. The calculated results are consistent with these observations.
4. The heat flux from the wall to the wall film increases with the increase in the wall temperature, and the calculations also reproduce this change well.
5. At the wall temperature of 60°C, the wall film of the gasoline surrogate fuel exhibits a very low vaporization rate, compared to that of pure iso-octane. This is because the highest boiling point component in the surrogate fuel remains unevaporated in the wall film. As aromatics are generally the higher boiling point components in gasoline, they are potential sources of pool fires and soot in DISI gasoline engines.

In order to additionally validate the calculated film formation and evaporation processes, at higher ambient pressure, further measurements should be planned.

Acknowledgements

This work was supported by Council for Science, Technology and Innovation (CSTI), Cross-ministerial Strategic Innovation Promotion Program (SIP), “Innovative combustion technology” (funding agency: JST).

References

[1] Stevens, E. and Steeper, R., Piston Wetting in an Optical DISI Engine: Fuel Films, Pool Fires, and Soot Generation, SAE Technical Paper, No.2001-01-1203 (2001).

[2] Drake, M., Fansler, T., Solomon, A. and Szekely, G., Piston Fuel Films as a Source of Smoke and Hydrocarbon Emissions from a Wall-Controlled Spark-Ignited Direct-Injection Engine, SAE Technical Paper, No.2003-01-0547 (2003).

[3] Naber, J. D. and Reitz, R. D., Modeling Engine Spray/Wall Impingement, SAE Technical Paper, No. 880107 (1988).

[4] Bai, C. and Gosman, A. D., Development of Methodology for Spray Impingement Simulation, SAE Technical Paper, No.950283 (1995).

[5] Stanton, D. W. and Rutland, C. J., Modeling Fuel Film Formation and Wall Interaction in Diesel Engines, SAE Technical Paper, No.960628 (1996).

[6] Mundo, C., Sommerfeld, M. and Tropea, C., Droplet-Wall Collisions: Experimental Studies of the Deformation and Breakup Process, Int. J. Multiphase Flow, Vol.21, No.2 (1995) 151-173.

[7] Köpple, F., Jochmann, P., Hettinger, A. and Kufferath, A., A Novel CFD Approach for an Improved Prediction of Particulate Emissions in GDI Engines by Considering the Spray-Cooling on the Piston, SAE Technical Paper, No.2015-01-0385 (2015).

[8] Kuhnke, D., Spray / Wall - Interaction Modeling by Dimensionless Data Analysis, Ph-D Thesis, University of Darmstadt (2004).

[9] Zhang, Y., Jia, M., Liu, H. and Xie, M., Development of an Improved Liquid Film Model for Spray/Wall Interaction under Engine-Relevant Conditions, Int. J. Multiphase Flow, Vol.79 (2016) 74-87.

[10] Senda, J., Kanda, T., Al-Roub, M., Farrell, P. V., Fukami, T. and Fujimoto, H., Modeling Spray Impingement Considering Fuel Film Formation on the Wall, SAE Technical Paper, No. 970047 (1997).

[11] Senda, J. and Fujimoto, H., Multidimensional Modeling of Impinging Sprays on the Wall in Diesel Engines, American Society of Mechanical Engineers, Applied Mechanical Review, Vol.52, No.4 (1999) 119-138.

[12] O’Rourke, P. J. and Amsden, A. A., A Particle Numerical Model for Wall Film Dynamics in Port-Injected Engines, SAE Technical Paper, No.961961 (1996).

[13] Jiao, Q. and Reitz, R. D., Modeling Soot Emissions from Wall Films in a Direct-Injection Spray-Ignition Engine, International Journal of Engine Research, Vol.16,

Issue 8, (2014) 994-1013.

[14] Kalghatgi, G., Fuel/Engine Interactions, Chapter 2, *SAE International* (2014)

[15] Jin, J. D. and Borman, G. L., A Model for Multicomponent Droplet Vaporization at High Ambient Pressures, SAE Technical Paper, No.850264 (1985).

[16] Ayoub, N. S. and Reitz, R. D., Multidimensional Computation of Multicomponent Spray Vaporization and Combustion, SAE Technical Paper, No.950285 (1995).

[17] Lippert, A. M. and Reitz, R. D., Modeling of Multicomponent Fuels Using Continuous Distributions with Application to Droplet Evaporation and Sprays, SAE Technical Paper, No.972882 (1997).

[18] Miyagawa, H., Nagaoka, M., Akihama, K. and Fujikawa, T., Numerical Analysis on Multi-Component Fuel Behaviors in a Port-Injection Gasoline Engine, SAE Technical Paper, No.1999-01-3642 (1999).

[19] Ra, Y. and Reitz, R. D., The application of a Multicomponent Droplet Vaporization Model to Gasoline Direct Injection Engines, International Journal of Engine Research, Vol.4, No.3 (2003) 193-218.

[20] Kawano, D., Senda, J., Wada, Y., Fujimoto, H., Goto, Y., Odaka, M., Ishii, H. and Suzuki, H., Numerical Simulation of Multicomponent Fuel Spray, SAE Technical Paper, No.2003-01-1838 (2003).

[21] Zhang, L. and Kong, S.-C., High-Pressure Vaporization Modeling of Multi-Component Petroleum-Biofuel Mixtures Under Engine Conditions, Combustion and Flame, Vol.158, Issue 9 (2011) 1705-1717.

[22] Hosain, M. L., Fdhila, R. B. and Daneryd, A., Heat Transfer by Liquid Jets Impinging on a Hot Flat Surface, Applied Energy, Vol.164 (2016) 934-943.

[23] Köpple, F., Jochmann, P., Kufferath, A. and Bargende, M., Investigation of the Parameters Influencing the Spray-Wall Interaction in a GDI Engine – Prerequisite for the Prediction of Particulate Emissions by Numerical Simulation, SAE Int. J. Engines 6 (2) (2013) 911-925.

[24] Schulz, F. and Beyrau, F., Systematic Investigation of Fuel Film Evaporation, SAE Technical Paper, No.2018-01-0310 (2018).

[25] Mizobuchi, Y., Development of Automotive Engine Combustion Simulation Software “HINOCA”, (written in Japanese) Journal of the Combustion Society of Japan, Vol.58, No.186 (2016) 191-196.

[26] Ducros, F., Nicoud, F. and Poinsot, T., Wall-Adapting Local Eddy-Viscosity Models for Simulations in Complex Geometries, Proceedings of the Conference on Numerical Methods for Fluid Dynamics (1998) 293-299.

[27] Beale, J. C. and Reitz, R. D., Modeling Spray Atomization with the Kelvin-Helmholtz/Rayleigh-Taylor Hybrid Model, Atomization and Sprays, Vol.9, Issue 6 (1999) 623-650.

[28] Tomoda, T., Kawauchi, M., Kubota, M., Nomura, Y. and Senda, J., Modeling of Wall Impinging Behavior with a Fan Shaped Spray, SAE Technical Paper, No.2003-01-1841 (2003).

[29] Al-Roub, M., Farrell, P. V. and Senda, J., Near Wall Interaction in Spray Impingement, SAE Technical Paper, No.960863 (1996).

[30] Ueda, T., Enomoto, T. and Kanematsu, M., Heat Transfer Characteristics and Dynamic Behavior of Saturated Droplets Impinging on a Heated Vertical Surface, Bulletin of the JSME, Vol.22, No.167 (1979) 724-732.

[31] Cossali, G. E, Coghe, A. and Marengo, M., The Impact of a Single Drop on a Wetted Solid Surface, Experiments in Fluids, Vol.22, Issue 6 (1997) 463-472.

[32] Mundo, C., Sommerfeld, M. and Tropea, C., Droplet-Wall Collisions: Experimental Studies of the Deformation and Breakup Process, International Journal of Multiphase Flow, Vol.21, No.2 (1995) 141-173.

[33] Kalantari, D. and Tropea, C., Spray Impact onto Flat and Rigid Walls: Empirical Characterization and Modeling, International Journal of Multiphase Flow, Vol.33, Issue 5 (2007) 525-544.

[34] Kobashi, Y., Kimoto, Y. and Kato, S., Experimental Validation of a Droplet Vaporization Model for Ethanol-Blended Fuels and its Application to Spray Simulation, SAE Technical Paper, No.2014-01-2733 (2014).

[35] Enomoto, Y. and Furuhama, S., Study on Thin Film Thermocouple for Measuring Instantaneous Temperature on Surface of Combustion Chamber Wall in Internal Combustion Engine, Bulletin of JSME, Vol.28, No.235 (1985) 108-116.

[36] Schulz, F. and Beyrau, F., The Effect of Operating Parameters on the Formation of Fuel Wall Films as a Basis for the Reduction of Engine Particulate Emissions, Fuel, Vol.238 (2019) 375-384.

[37] Schulz, F., Schmidt, J., Kufferath, A. and Samenfink, W., Gasoline Wall Films and Spray/Wall Interaction Analyzed by Infrared Thermography, SAE Int. J. Engines 7(3) (2014) 1165-1177.

[38] Senda, J., Higaki, T., Sagane, Y., Fujimoto, H., Takagi, Y. and Adachi, M., Modeling and Measurement on Evaporation Process of Multicomponent Fuels, Journal of Engines, Vol.109, Section 3 (2000) 347-358.

[39] Friend, D. G. and Huber, M. L., Thermophysical Property Standard Reference Data from NIST, International Journal of Thermophysics, Vol.15, No.6 (1994) 1279-1288.

[40] Peng, D.-Y. and Robinson, D. B., A New Two-constant Equation of State, Ind. Eng. Chem. Fundam., Vol.15, No.1 (1976) 59-64.

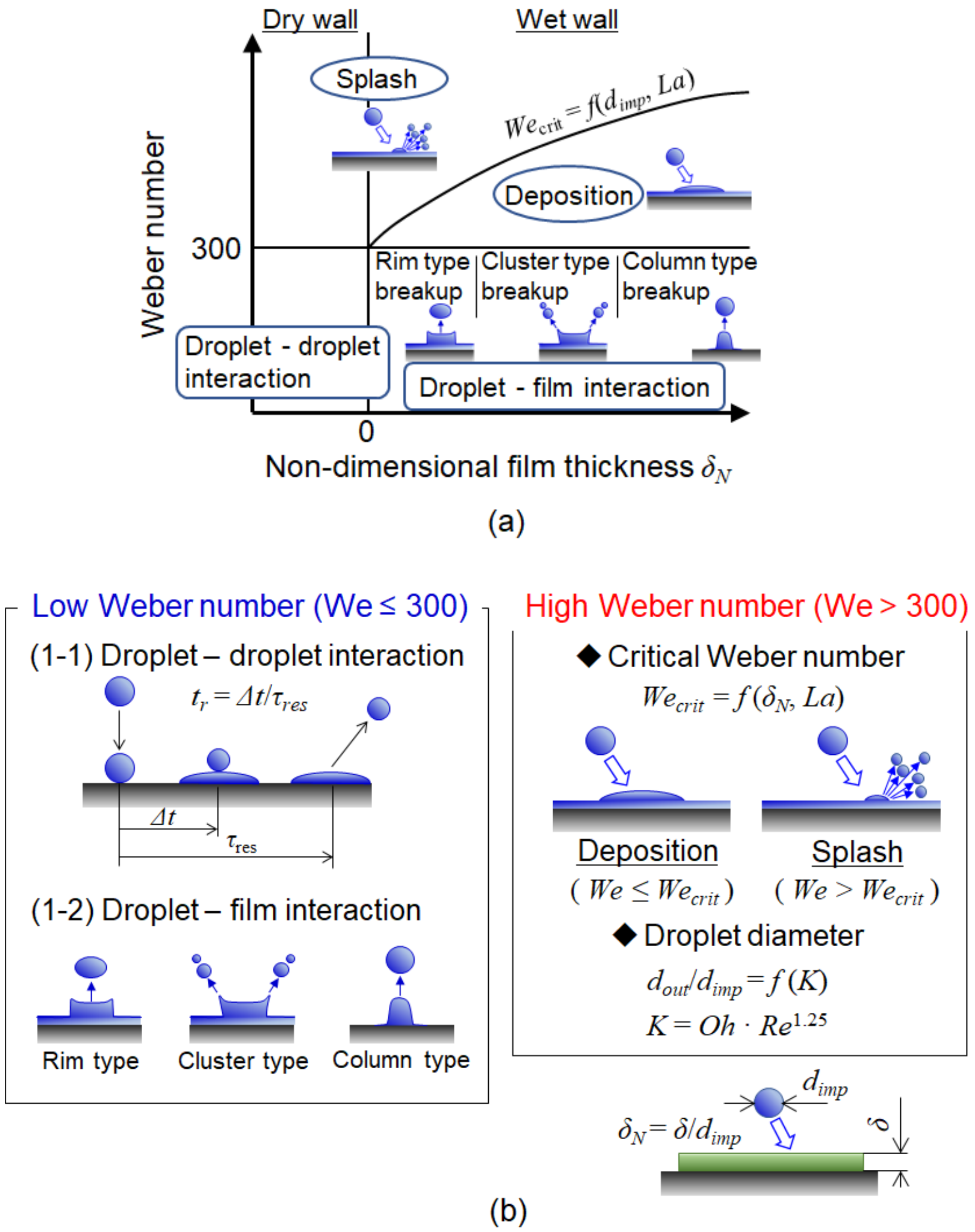

Fig.1 Droplet / wall impingement model proposed by Senda [10-11]

(a) classification of impinging droplet behavior with Weber number and non-dimensional film thickness

(b) droplet impingement model for low and high Weber numbers

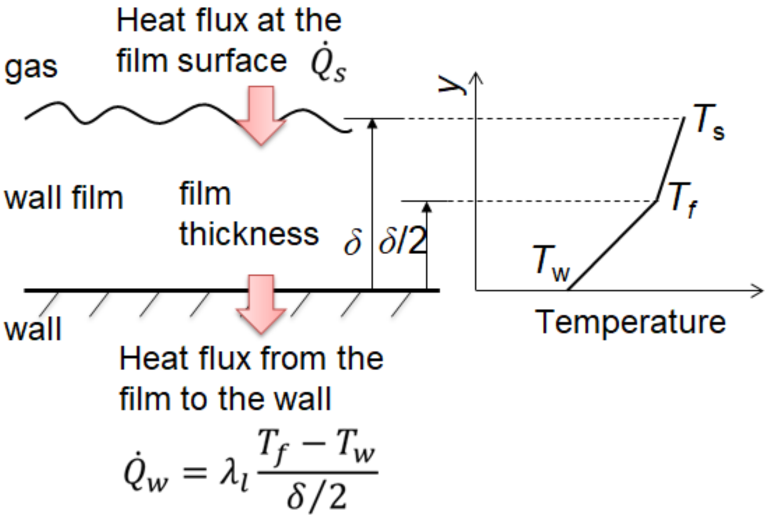

Fig.2 Illustration of the heat transfer and linear temperature assumptions in the wall film model [12]

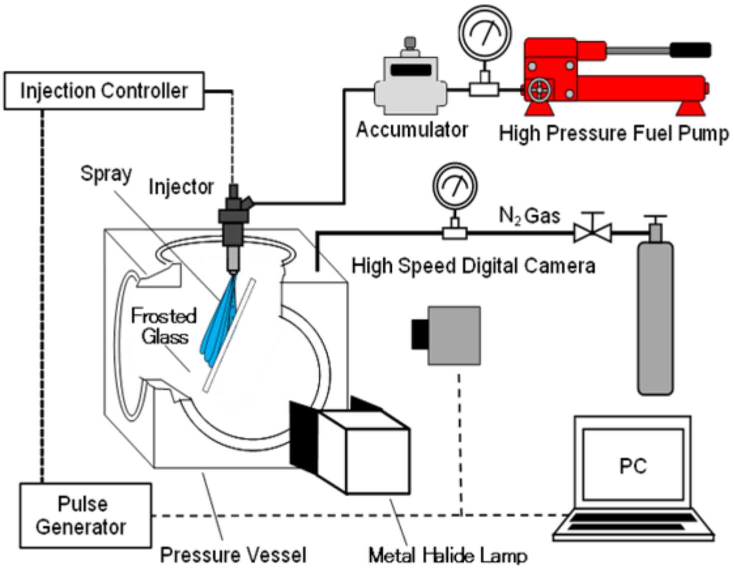

Fig.3 Experimental setup for film area measurements

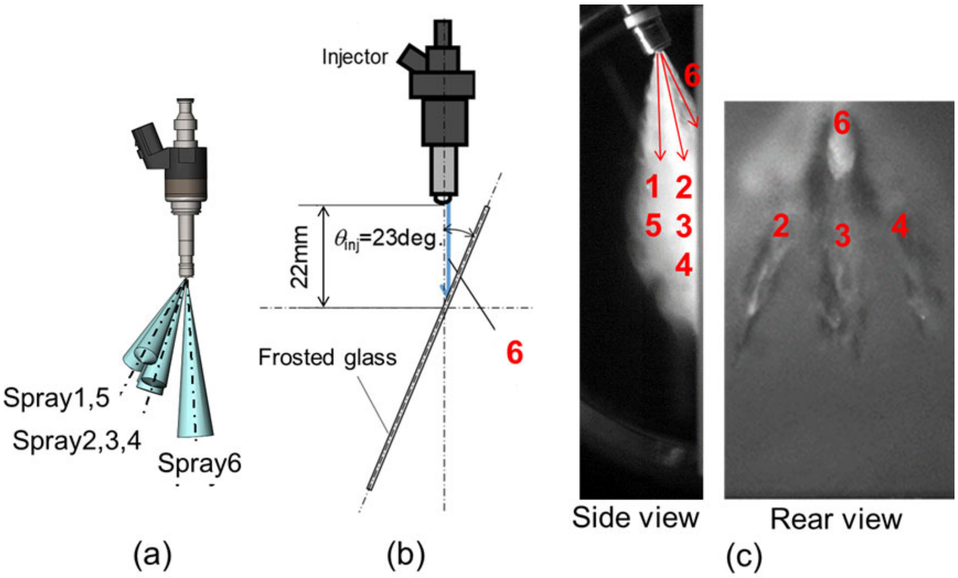

(a) (b) (c)

Fig.4 (a) & (b) Arrangement of the fuel sprays for the film area measurements and (c) images of recorded spray tracks

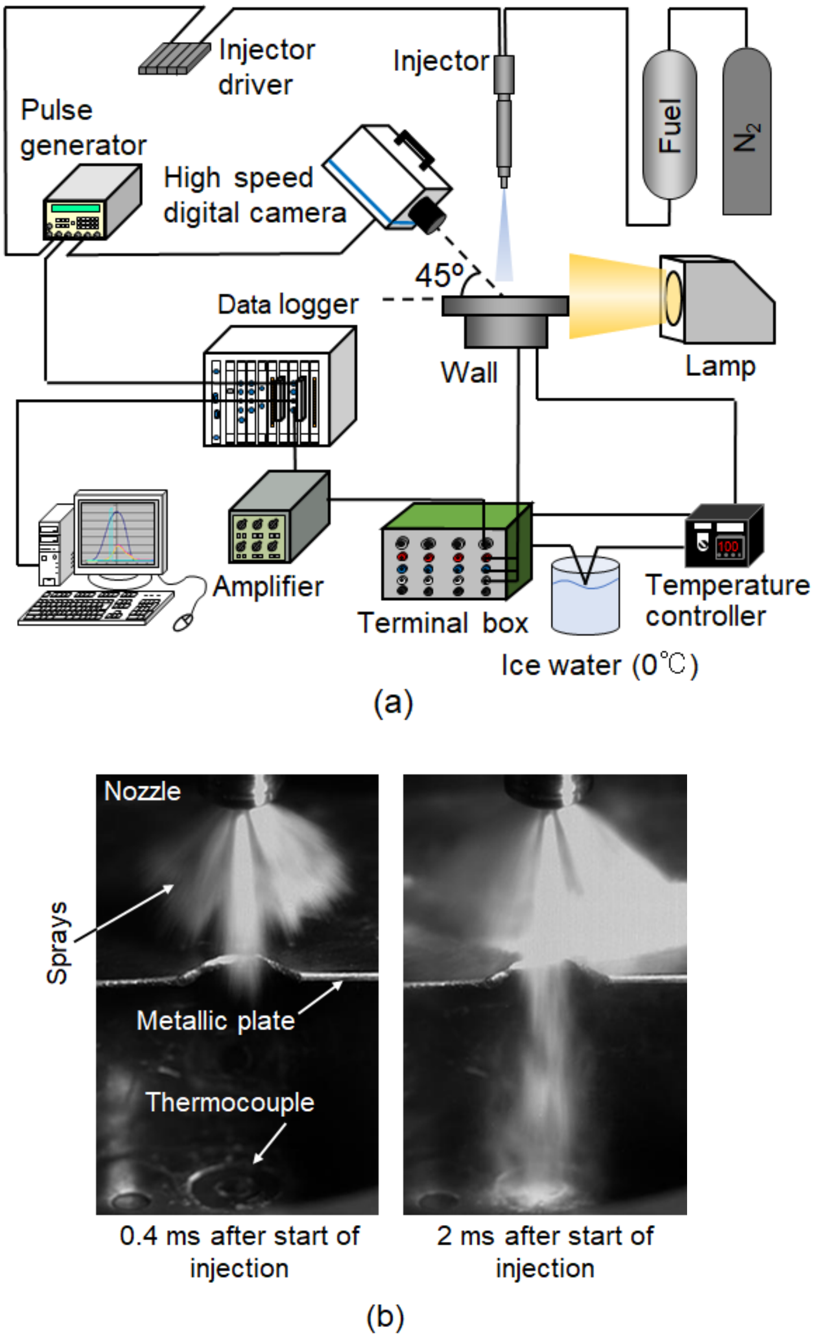

Fig.5 Experimental setup for visualization of the wall film and measurements of the wall heat flux

(a) overall system

(b) layout of the fuel sprays and thermocouple

(one spray orthogonally impinged on the thermocouple while the other sprays were masked with the metallic plate)

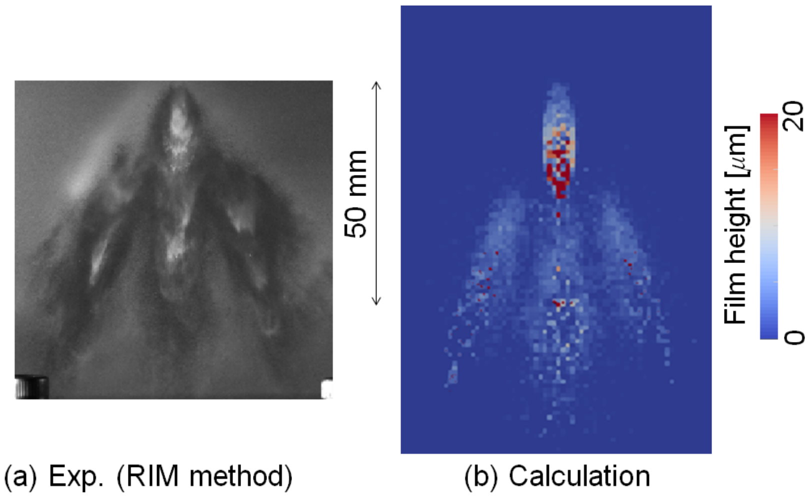

(a) Exp. (RIM method) (b) Calculation

Fig.6 Wall film images (a) taken with RIM method and (b) calculated (p_{inj} = 13 MPa, T_w = 20°C)

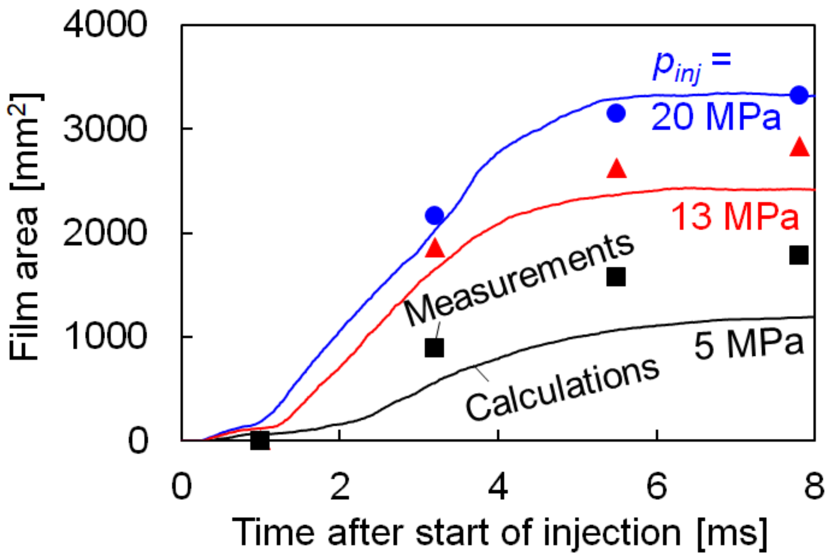

Fig.7 Plots of wall film areas for the measurements and calculations (T_w = 20°C)

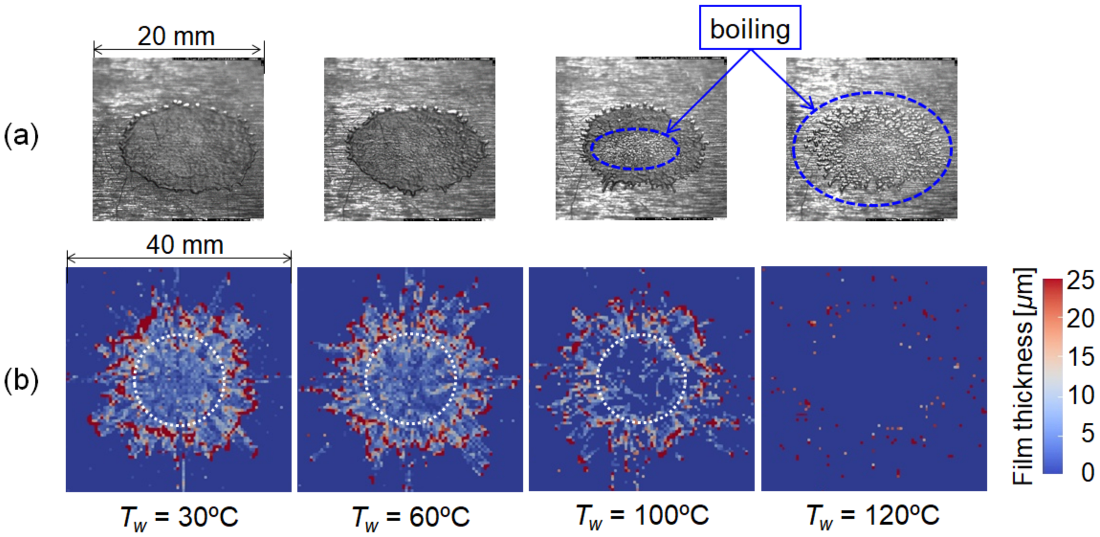

Fig.8 Images of the (a) photographed and (b) calculated wall films at different wall temperatures T_w

Dashed white lines equivalent to the measured wall film diameters are superimposed on (b) (t_inj = 7 ms)

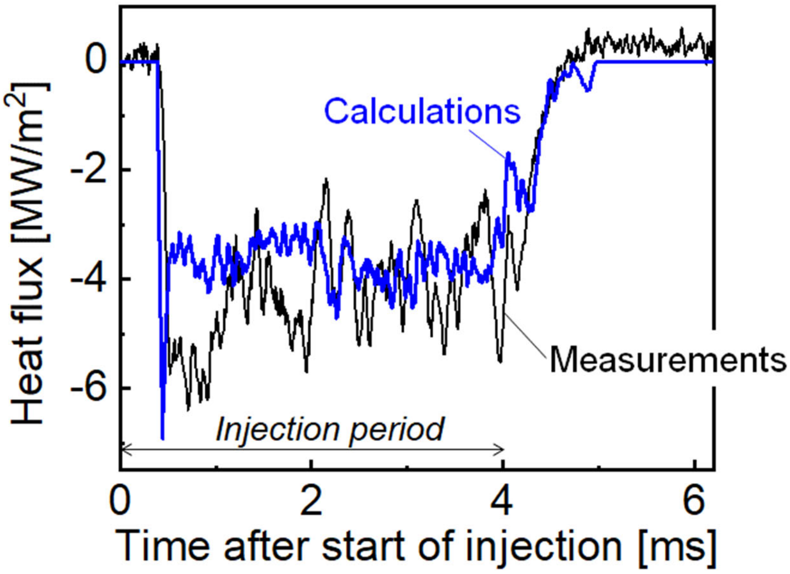

Fig.9 Plot of profiles of the heat flux for the measurements and calculations (T_w = 120°C)

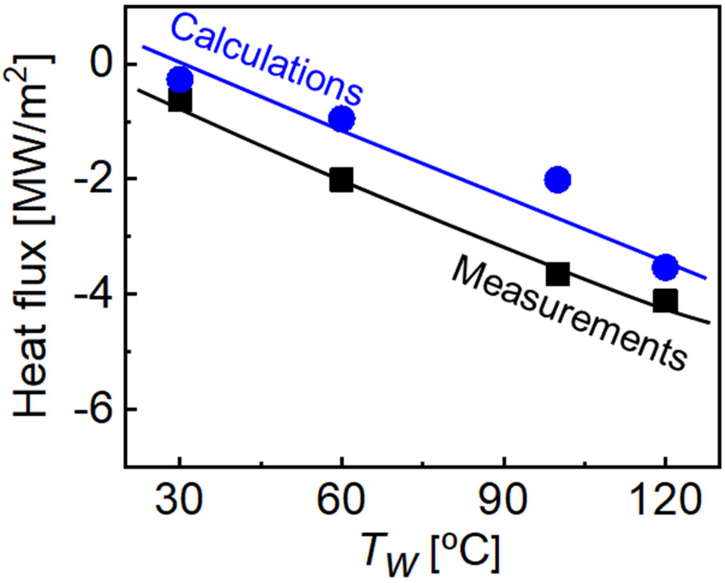

Fig.10 Plot of the changes in the heat flux versus the wall temperature T_w for the measurements and calculations

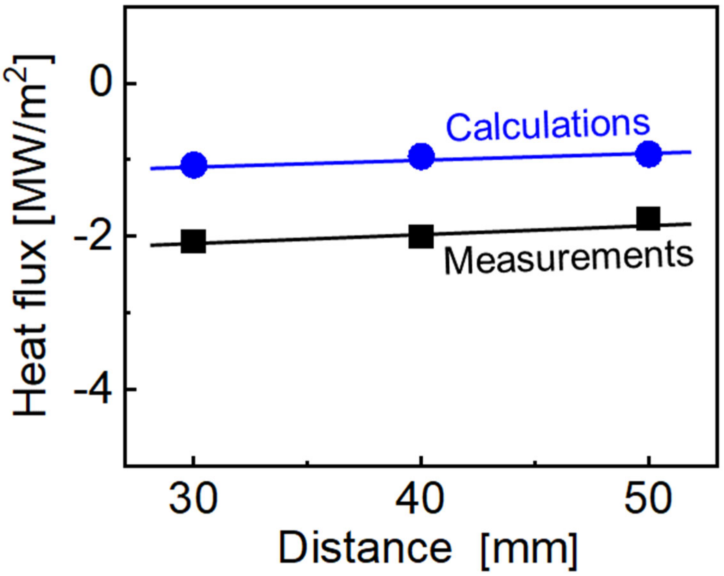

Fig.11 Plot of the changes in the heat flux versus the distance from injection nozzle to wall for the measurements and calculations

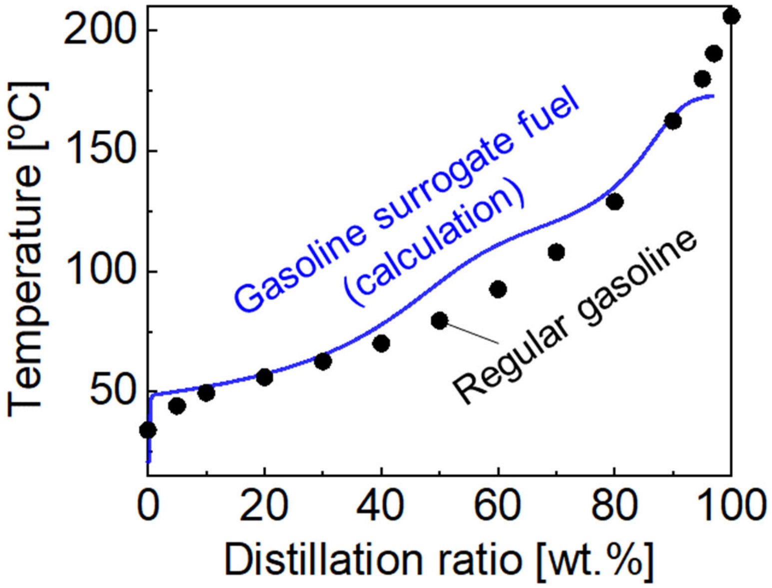

Fig.12 Plot of the temperature versus distillation ratio curves for the gasoline surrogate fuel and regular gasoline

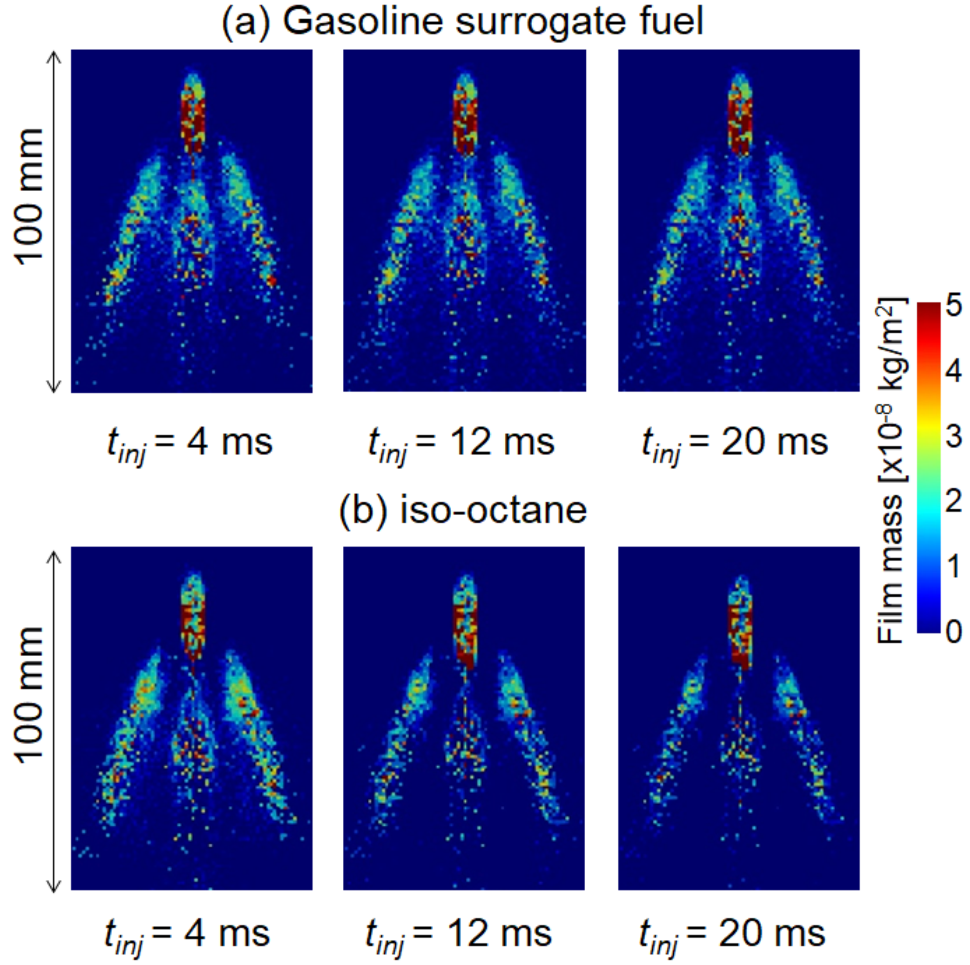

Fig.13 Calculated film thickness distributions of (a) the gasoline surrogate fuel and (b) iso-octane (T_w = 60°C)

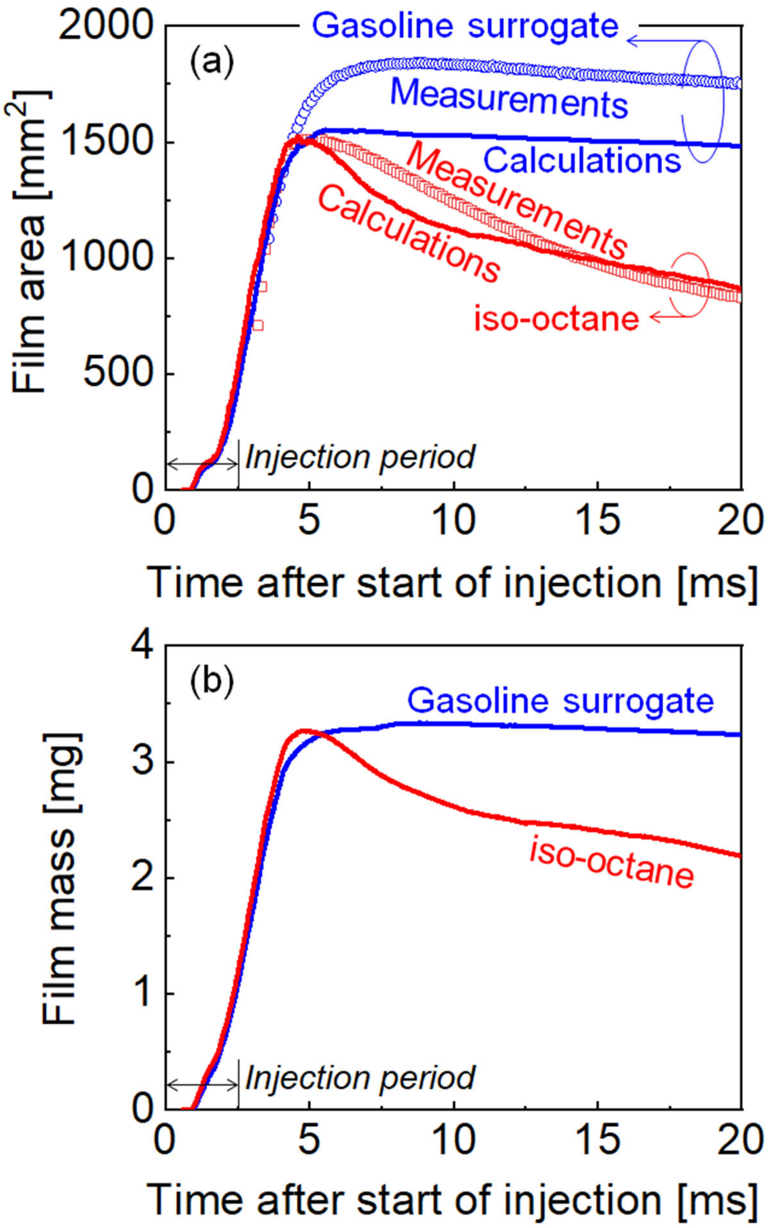

Fig.14 Plots of (a) the measured and calculated film areas and (b) the calculated mass of the wall film of the gasoline surrogate fuel and iso-octane (T_w = 60°C)

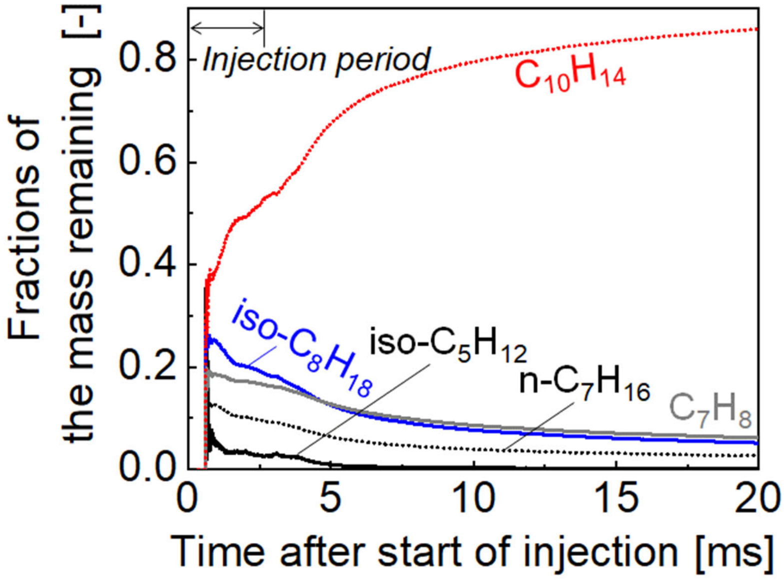

Fig.15 Calculated profiles of the mass fraction of the components present in the wall film of the gasoline surrogate fuel (T_w = 60°C)

Table 1 Conditions for the film area measurements and calculations with iso-octane

Ambient pressure	[MPa]	0.10
Ambient temperature	[ºC]	20
Wall temperature, T_w	[ºC]	20
Nozzle diameter	[mm]	0.13
Injection pressure	[MPa]	5, 13, 20
Injection period	[ms]	2.5
Fuel		iso-octane (C_8H_{18})

Table 2 Conditions used in evaluating the wall heat flux of iso-octane

Ambient pressure	[MPa]	0.10
Ambient temperature	[ºC]	20
Wall temperature, T_w	[ºC]	30, 60, 100, 120
Nozzle diameter	[mm]	0.248
Injection pressure	[MPa]	10
Injection period	[ms]	4
Impinging distance	[mm]	30, 40, 50
Impinging angle	[º]	90
Total Injection quantity	[mg]	109
Fuel		iso-octane (C_8H_{18})

Table 3 Gasoline surrogate fuel proposed in the present study

(a) boiling point and RON of single component fuels and their mixing fraction

(b) properties of gasoline surrogate fuel, compared with regular gasoline referenced

(a)

	Boiling point [°C]	RON [-]	Volume fraction [vol.%]	Mass fraction [wt.%]
iso-pentane (C_5H_{12})	28.0	96	45	39
n-heptane (C_7H_{16})	98.4	0	10	10
iso-octane (C_8H_{18})	99.3	100	20	20
Toluene (C_7H_8)	110.6	111	10	12
1,2,4-trimethylbenzene (C_9H_{12})*	169.4	108	15	19

* replaced by iso-butylbenzene ($C_{10}H_{14}$) in the present study

(b)

	Gasoline surrogate fuel	Reference regular gasoline
RON [-]	90.5	90.8
Aromatic content [vol.%]	25.0	25.4
Density [kg/m^3]	711	730
Viscosity [μPa·s]	404	N/A